Since January 2020 Elsevier has created a COVID-19 resource centre with free information in English and Mandarin on the novel coronavirus COVID-19. The COVID-19 resource centre is hosted on Elsevier Connect, the company's public news and information website.

Elsevier hereby grants permission to make all its COVID-19-related research that is available on the COVID-19 resource centre - including this research content - immediately available in PubMed Central and other publicly funded repositories, such as the WHO COVID database with rights for unrestricted research re-use and analyses in any form or by any means with acknowledgement of the original source. These permissions are granted for free by Elsevier for as long as the COVID-19 resource centre remains active.

Cell Chemical Biology

Bioorthogonal dissection of the replicase assembly of hepatitis C virus

Graphical abstract

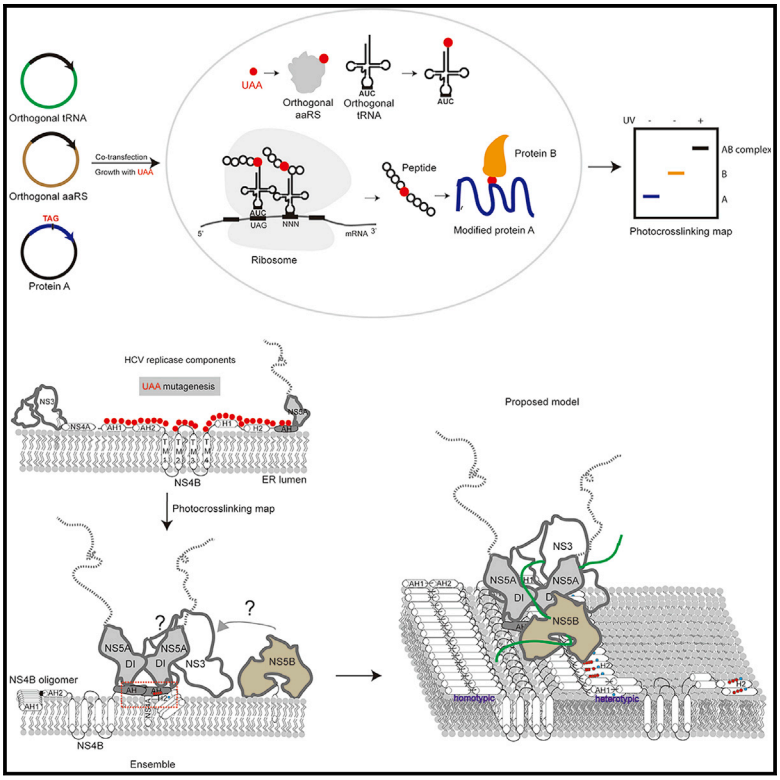

Highlights

- N-terminal AH1 and C-terminal residue L237 mainly mediate NS4B oligomerization
- NS4B C-terminal residues S227, D228, A229, and R232 are the docking sites of NS3
- NS5A AH plays a role in NS5A-NS4B interaction and NS5A dimerization
- NS4B C-terminal H2 and NS5A AH are hub elements in HCV replicase assembly

Authors

Yang Zhang, Shuiye Chen, Zhenghong Yuan, Zhigang Yi

Correspondence

zhyuan@shmu.edu.cn (Z.-H.Y.), zgyi@fudan.edu.cn (Z.-G.Y.)

In brief

Zhang et al. use a polyprotein expression model to introduce a photoactivatable unnatural amino acids at individual residues to characterize the interaction between HCV replicase components NS4B, NS5A, and NS3. The detailed landscape of protein-protein interactions provides a model for replicase assembly.

Zhang et al., 2021, Cell Chemical Biology *28*, 1366–1378
September 16, 2021 © 2021 Elsevier Ltd.
https://doi.org/10.1016/j.chembiol.2021.03.006

CellPress

CellPress

Cell Chemical Biology

Resource

Bioorthogonal dissection of the replicase assembly of hepatitis C virus

Yang Zhang,[1] Shuiye Chen,[1] Zhenghong Yuan,[1,*] and Zhigang Yi[1,2,3,*]

[1]Key Laboratory of Medical Molecular Virology (MOE/NHC/CAMS), School of Basic Medical Sciences, Shanghai Medical College, Fudan University, Shanghai 200032, China

[2]Shanghai Public Health Clinical Center, Fudan University, Shanghai 201052, China

[3]Lead contact

*Correspondence: zhyuan@shmu.edu.cn (Z.-H.Y.), zgyi@fudan.edu.cn (Z.-G.Y.)

https://doi.org/10.1016/j.chembiol.2021.03.006

SUMMARY

Positive-strand RNA viruses such as hepatitis C virus (HCV), flaviviruses, and coronaviruses are medically important. Assembly of replicase on host membranes is a conserved replication strategy and an attractive antiviral target. The mechanisms of replicase assembly are largely unknown, due to the technical difficulties in purifying the replicase and carrying out structural studies. Here, with an HCV replicase assembly surrogate system, we employed a bioorthogonal system to introduce the photolabile unnatural amino into each residue in the cytosolic regions of NS4B and the amphipathic helix (AH) of NS5A. Photocrosslinking enabled visualization of NS4B oligomerization and NS5A dimerization at pinpointed interacting residues and identifying contacting sites among the replicase components. Characterization of the interacting sites revealed hub elements in replicase assembly by docking replicase components to prompt protein-protein interactions. The results provide information about the molecular architecture of the replicase, advancing understanding of the mechanism of replicase assembly.

INTRODUCTION

Positive-strand RNA viruses include many public health-related pathogens, such as hepatitis C virus (HCV), which causes liver cirrhosis and liver cancer (Manns et al., 2017); Zika virus (Petersen et al., 2016); and severe acute respiratory syndrome coronavirus-2 (SARS-CoV-2), which has caused the ongoing coronavirus disease 2019 (COVID-19) pandemic. There is a scarcity of effective direct antiviral agents against these viruses, except for HCV, which can be cured by combinations of direct antiviral agents (Kohli et al., 2014). Positive-strand RNA viruses share a conserved replication strategy. Viral nonstructural (NS) proteins assemble a membrane-associated replicase on host membranes, which induces modification of host membranes to form replication complex (RC) (den Boon and Ahlquist, 2010). Direct antiviral agents of HCV, the NS5A inhibitor daclatasvir and daclatasvir-like inhibitors (Gao et al., 2010), prevent the formation of the viral RC (Berger et al., 2014), probably by disrupting the replicase quaternary structure (Zhang et al., 2019b), highlighting the availability of replicase assembly as an antiviral target. Determining the molecular mechanism of the replicase assembly may inspire the development of novel direct antiviral agents. Recently, by using cryo-EM tomography, Paul Ahlquist and coworkers reported the structure of nodavirus replicase, which is assembled solely by the replication protein A (Unchwaniwala et al., 2020). However, determining the structure of a multicomponent replicase remains technically challenging, largely due to the difficulties in purifying the whole replicase, which usually has a low abundance and is associated with host factors (Yi et al., 2016).

HCV is a member of the Flaviviridae family. Its 9.6-kb positive-sense RNA genome encodes a polyprotein that is co- and post-translationally processed to produce the viral structural proteins and nonstructural proteins NS2, NS3, NS4A, NS4B, NS5A, and NS5B (see Moradpour et al., 2007 for review). NS3 contains a protease domain in the N-terminal region, which uses NS4A as a cofactor, and an RNA helicase/NTPase domain in the C-terminal region. NS4B is a multispanning integral membrane protein, and its oligomerization is required for viral replicase assembly. NS5A has nonenzymatic activity and plays a central role in viral replicase assembly. NS5A has an amphipathic helix (AH) at the amino terminus, which was suggested to mediate membrane anchoring and was recently demonstrated to regulate polyprotein processing and protein-protein interactions within the replicase (Zhang et al., 2019a). NS5B is the viral RNA-dependent RNA polymerase (see Gu and Rice, 2013 for a review). NS3, NS4A, NS4B, NS5A, and NS5B assemble the viral replicase on the ER forming a double-membrane vesicle (Romero-Brey et al., 2012), but the underlying molecular mechanisms remain largely unknown.

In this study, we used a viral replicase assembly surrogate system wherein the HCV NS3-5B polyprotein is expressed to mimic the induction of viral replicase assembly (Romero-Brey et al., 2012). We focused on the NS4B and NS5A proteins that play

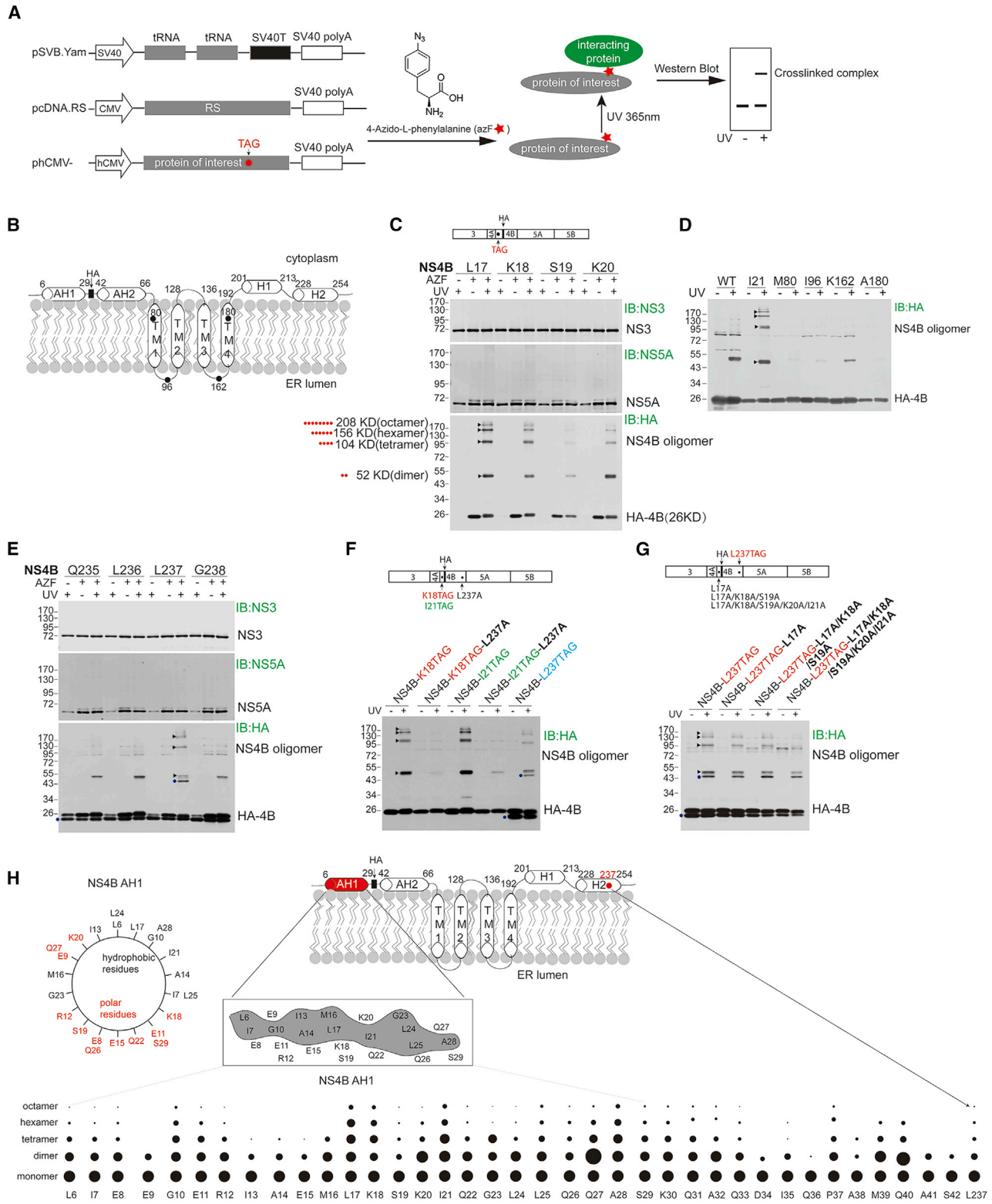

Figure 1. Identification of self-interacting residues in the NS4B oligomers by photocrosslinking

(A) Experimental design of *in vivo* photocrosslinking.

(B) Schematic of NS4B membrane topology. The N-terminal amphipathic helices AH1 and AH2, the four transmembrane helices (TM1 to TM4), and the C-terminal helices H1 and H2 are indicated. Residues are numbered. Black box, HA tag.

(legend continued on next page)

central roles in assembling the HCV replicase (Egger et al., 2002; Paul et al., 2011; Romero-Brey et al., 2012). We employed a bioorthogonal strategy in which amber suppressor tRNA/aminoacyl-tRNA synthetase (aaRS) pair is orthogonal to mammalian tRNAs and synthetases and unnatural amino acids (UAAs) such as photolabile UAA p-azido-L-phenylalanine (azF) can be introduced by the orthogonal pair into the amber codon (UAG) during protein translation. Upon UV illumination, azF can form highly reactive nitrone that undergoes ring expansion and nucleophile addition, initiating chemical crosslinking to neighboring primary amines or aliphatic hydrogens (Huber and Sakmar, 2014). This crosslinking typically occurs only within the side chains of an interacting pair at a distance range of 3–4 Å (Sato et al., 2011) and results in a specific covalent bond, which provides positional information on the protein-protein interactions and protein contacts within a complex at the atomic level. We introduced azF into the residues in the cytosolic regions of NS4B and NS5A AH. By photocrosslinking, we dissected the interacting maps of pinpointed residues of the replicase components. We defined the contacting residues in NS4B oligomers. We detected NS5A dimer *in vivo* and uncovered that domain I and the N-terminal AH reciprocally regulated NS5A dimerization. Photocrosslinking among the viral replicase components identifies hub elements in replicase assembly by docking replicase components to prompt the NS3-NS4B-NS5A interaction.

RESULTS

Establishment of a bioorthogonal system for investigating HCV replicase assembly

We employed a bioorthogonal system using the orthogonal suppressor tRNA/aminoacyl-tRNA synthetase (aaRS) pair for the photolabile UAA p-azido-L-phenylalanine (azF) (Naganathan et al., 2013). We cotransfected cells with plasmids expressing the suppressor tRNA and aaRS and plasmid expressing proteins of interest (protein A) with an amber codon (TAG) at desired positions. AzF is incorporated into the amber codon (TAG) by the suppressor tRNA and the aminoacyl-tRNA synthetase when the cells are grown in media with azF, resulting in a protein variant with azF at the specific amino acid position where the TAG is introduced. Upon UV illumination, contacting of an interacting protein (protein B) with protein A that is near enough mediates a cross link, which allowed us to detect the covalent protein A-B by denaturing SDS-PAGE and western blotting (Figure 1A). Thus, we can determine the location of the residues in protein A that contacts with protein B and involved in their interaction *in vivo*.

We first verified photocrosslinking of the glutathione S-transferase (GST) dimer. We introduced the TAG stop codon into residue V125 based on the structure of the GST dimer (Figure S1A). We cotransfected HEK293T cells with plasmids pSVB.Yam and pcDNA.RS and plasmid expressing HA-tagged GST with V125TAG mutation. AzF was readily incorporated into GST, resulting in the expression of full-length GST. Upon UV illumination, substantial GST dimers were detected by SDS-PAGE and western blot analyses (Figure S1B), suggesting efficient photocrosslinking of the GST dimer via azF at residue 125.

Then, we sought to use the bioorthogonal system to dissect the interactome of the replicase. We first used this system to verify the interaction of NS5A with the reported host factor MOB1b (Chung et al., 2014). Based on the cocrystal structure of MOB1b and a peptide of NS5A, we introduced TAG in the residues W312, Y317, and V322 of NS5A in the context of NS3-5B, with an HA tag inserted into a viral replication-tolerant site in domain III of NS5A (Yi et al., 2016; Zhang et al., 2019b) (Figure S1C). We detected the photocrosslinked MOB1b-NS5A complex via residue V322-mediated crosslinking (Figure S1D). These results demonstrate that this bioorthogonal system can be used for studying protein-protein interactions in replicase assembly surrogate systems.

Identification of self-interacting residues in the NS4B oligomers by photocrosslinking

NS4B is a multispanning membrane protein. It contains four transmembrane (TM) helices, two amphipathic helices AH1 and AH2 (Paul et al., 2011) in the N terminus, and two α-helices H1 and H2 in the highly conserved C-terminal region (Gouttenoire et al., 2010a). AH2 has been reported to mediate oligomerization of NS4B by using a fluorescence resonance energy transfer (FRET) method (Gouttenoire et al., 2010b). With a similar method, it has been demonstrated that the C-terminal H1 mediates NS4B self-interaction (Paul et al., 2011). The C-terminal H2 is also an AH that mediates the membrane association of NS4B (Gouttenoire et al., 2009). As the viral replicase assembles on the cytoplasmic side of the ER we introduced TAG in each residue of the cytosolic regions of NS4B, including the N-terminal region, the cytosolic loop, and the C-terminal region (Figure 1B), although NS4B adopts an alternative topology with AH1 translocated into the ER lumen (Lundin et al., 2006). To facilitate

(C) HEK293T cells were cotransfected with the plasmid pSVB.Yam, pcDNA.RS, and HCV NS3-5B-4B^{HA}-NS4B mutants with TAG introduced in the indicated amino acids. After photocrosslinking, cell lysates were analyzed by western blot. IB, immune blot. Arrows and red dots indicate NS4B oligomers with the expected molecular weights (kD).

(D) Photocrosslinking of amino acids in the transmembrane helices and loops (indicated in B, dots). Arrows indicate NS4B oligomers.

(E) Photocrosslinking of amino acids in the C-terminal helix H2. Arrows indicate NS4B oligomers. Blue dots indicate the non-azF-incorporated proteins whose translation stopped at the indicated TAG.

(F) L237 in the C-terminal helix H2 is required for NS4B oligomerization. TAG was introduced in the K18 or I21 sites of NS4B with the L237A mutation. Arrows indicate NS4B oligomers. Blue dots indicate the non-azF-incorporated proteins.

(G) Effect of the N-terminal amphipathic-helix AH1 mutations on L237-mediated NS4B oligomerization. Mutations were introduced in the N-terminal amphipathic-helix AH1 region of NS4B with L237TAG (red). Arrows indicate NS4B oligomers. Blue dots indicate the non-azF-incorporated proteins.

(H) Summary of the NS4B photocrosslinking results. The upper panel shows the schematic representation of NS4B AH1. The amino acids of NS4B AH1 from amino acids 6 to 29 on the α-helical wheel or in the N-terminal to C-terminal direction are shown. The hydrophobic face of the helix is shaded in gray. The bottom panel shows the NS4B oligomers mediated by NS4B AH1 and H2 L237. The abundance of each NS4B oligomer was quantified and normalized to the intensity of the monomer in the same lane. The intensities were plotted as dots with specific area. The area of each dot represents the intensity of the specific oligomer.

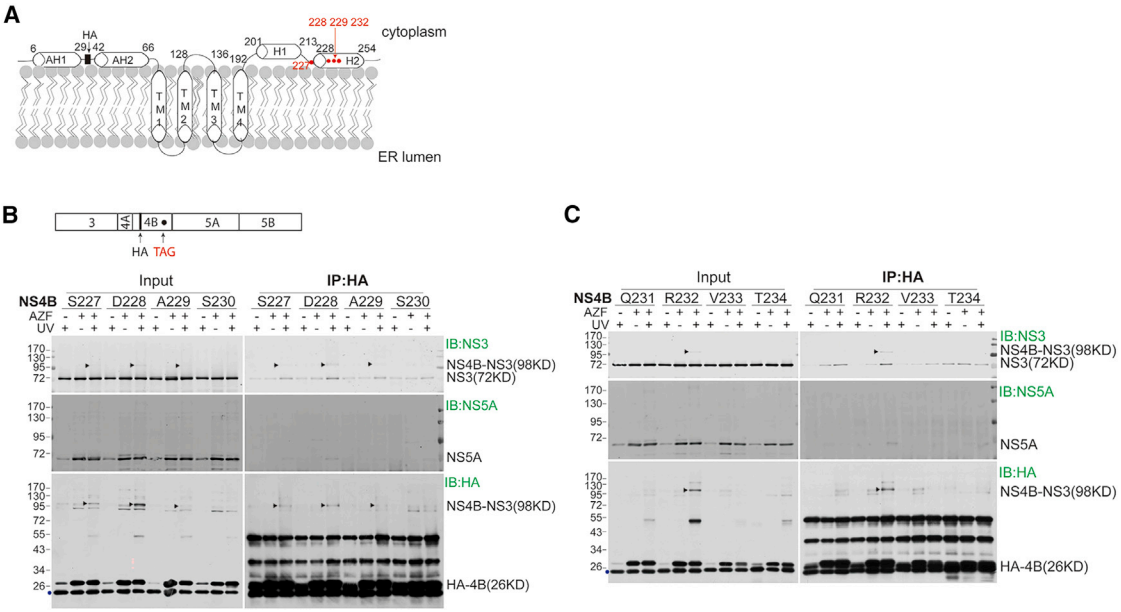

Figure 2. Identification of NS3-interacting sites on NS4B

(A) Schematic of NS4B membrane topology.

(B and C) Photocrosslinking of NS4B mutants in the backbone of NS3-5B-4B^{HA}. TAG (red) was introduced in the indicated amino acid sites of NS4B. After crosslinking and immunoprecipitation (IP) with an antibody against HA, proteins were analyzed by western blotting. Arrows indicate crosslinked protein complexes. Blue dots on the left indicate the non-azF-incorporated proteins.

detection and immunoprecipitation, an HA tag was inserted in a viral replication-tolerant site between residues 38 and 39 with a compensatory mutation Q31R, which is required to restore replication competence (Paul et al., 2013) (Figure 1B).

The series of site-specific azF mutants were efficiently translated and readily detected by anti-HA antibodies (Figures 1C and S2–S6). Upon UV illumination, NS4B-specific bands with molecular weights equivalent to the dimer, tetramer, hexamer, and octamer were detected in mutants of AH1 such as A1, S2, R3, A4, A5, L6, I7, E8, E9, G10, Q11, R12, I13, A14, E15, M16, L17, K18, K20, I21, Q22, Q23, L24, L25, Q26, Q27, and A28, and mutants such as S29, K30, Q31, A32, Q33, D34, I35, Q36, P37, M39, and Q40 in the linker region between AH1 and AH2 (Figures 1C and S2–S6), suggesting that these residues are contacting sites or self-interacting residues of NS4B in NS4B oligomers. In contrast, we could not detect obvious oligomers, except for the dimer, in residues M80 and A180 in transmembrane helices and I96 and K162 in the loops in the ER lumen (Figures 1B and 1D). Additionally, we detected crosslink via residue L237 in the C-terminal α-helix H2 (Figure 1E). These results demonstrate that residues in the N-terminal region and residue L237 in the C-terminal region are the contacting residues or self-interacting sites in the oligomerized NS4B (Figure 1H). It was noted that the dimer but not oligomers of NS4B was detected in the wild-type (WT) upon UV illumination, independent of azF (Figure 1D), which indicates that the dimer of NS4B is readily photocrosslinked, probably via certain photoactive natural amino acids. Next, we explored the interplay of the N-terminal self-interacting residues with the C-terminal self-interacting residue L237. We first selected K18 and I21 in the N-terminal AH1 for azF incorporation and then examined the effect of the L237A mutation on NS4B oligomerization via these two residues. We found that the L237A mutation abolished the dimerization and oligomerization of NS4B via K18 and I21 (Figure 1F). Then, we introduced single (L17A), triple (L17A, K18A, S19A), and quintuple (L17A, K18A, S19A, K20A, I21A) mutants in the N-terminal regions and examined their effects on oligomerization via L237; we observed that these mutants did not affect L237-mediated oligomerization (Figure 1G). These results suggest that L237-mediated self-interaction is a prerequisite for NS4B oligomerization.

Identification of NS3-interacting sites on NS4B

There is a strong interaction between NS3 and NS4B elucidated by means of immunoprecipitation (Zhang et al., 2019b), while the interacting sites are unknown. Using the azF-NS4B variants, we attempted to identify the NS3-interacting sites of NS4B. In the azF-NS4B variant-expressing cells, upon UV illumination, HA-NS4B was captured with anti-HA beads, and the immunoprecipitated complex was analyzed by SDS-PAGE and western blot with antibodies against NS3 and NS5A. In the azF-NS4B variants S227, D228, A229, and R232, crosslinked protein complexes with molecular weights equivalent to NS4B-NS3 were detected in the anti-HA-NS4B blot as well as in the anti-NS3 blot but not in the rest of the other azF-NS4B variants (arrows, Figures 2A–2C and S2–S6). These data indicate that S227, D228, A229, and R232 are NS3-interacting sites of NS4B or the docking sites of NS3 on NS4B.

Detection of NS5A dimerization *in vivo*

Except for the N-terminal AH, HCV NS5A has three domains. Domain I (DI) mediates NS5A dimerization. Poorly folded domain II (DII) and domain III (DIII) regulate viral genome replication

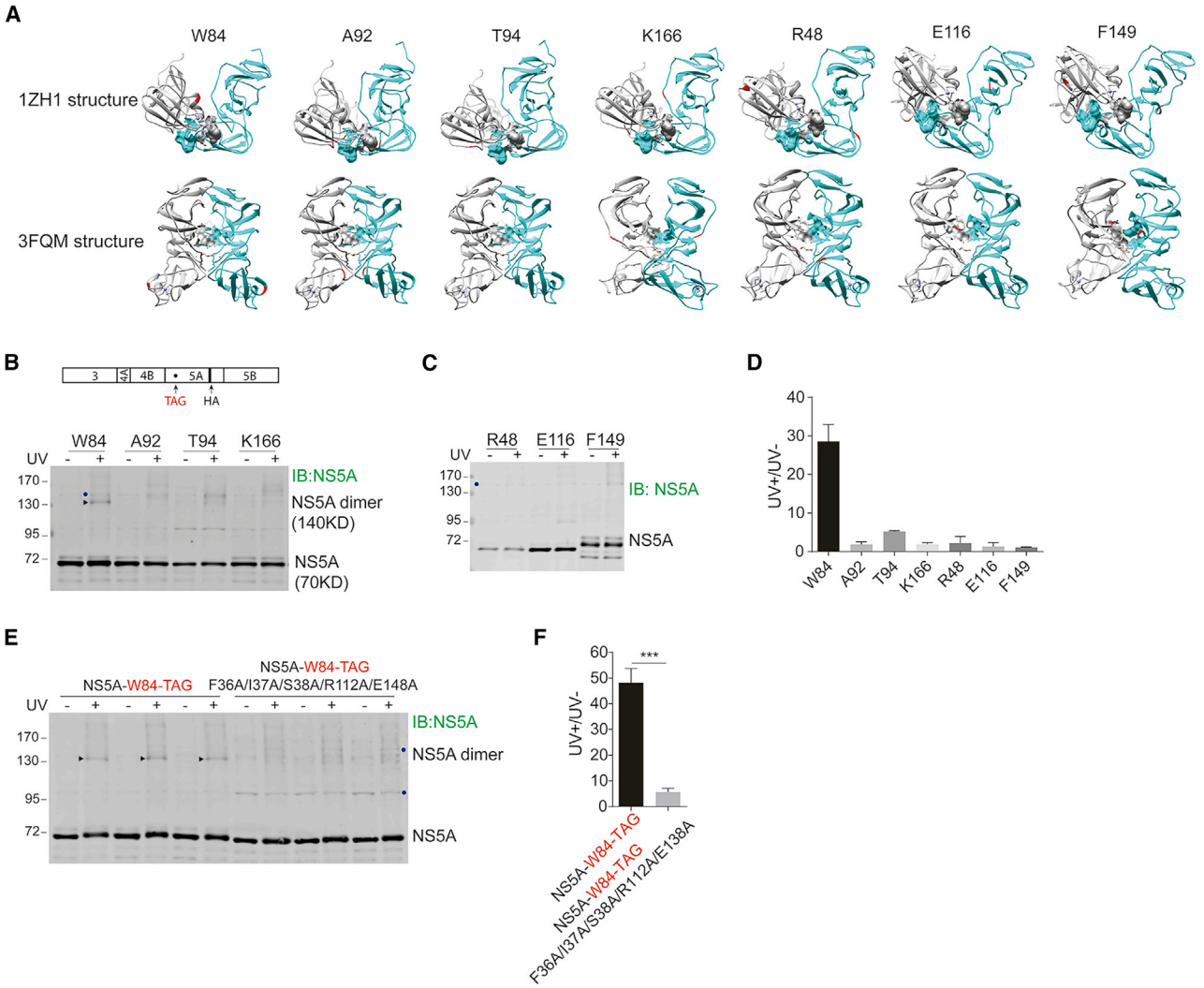

Figure 3. NS5A dimerization *in vivo*

(A) Crystal structure of the NS5A dimer (PDB: 1ZH1, 3FQM) with sites (in red) for azF incorporation.

(B and C) Photocrosslinking of NS5A mutants in the backbone of NS3-5B-5A^{HA}. TAG (red) was introduced in the indicated sites of NS5A. Arrows, NS5A dimer. Blue dots, nonspecific bands.

(D) The abundance of the NS5A dimer in (B) and (C) was quantified, and the intensity of the NS5A dimerization was calculated by the ratio of the band after UV exposure to that before UV treatment. Mean values ± SDs are shown (n = 3).

(E) Photocrosslinking of NS5A-W84-TAG. A combination of mutations that disrupt the NS5A dimer interface was introduced in NS5A with W84-TAG (red). Arrows, NS5A dimer. Blue dots, nonspecific bands.

(F) The abundance of the NS5A dimer in (E) was quantified, and the intensity of the NS5A dimerization was calculated by the ratio of the band after UV exposure to that before UV treatment. Mean values ± SDs are shown (n = 3). Statistical analysis was performed between NS5A-W84-TAG and the variant as indicated. ***$p < 0.001$, two-tailed, unpaired t test.

(Dujardin et al., 2015; Ross-Thriepland et al., 2013) and virion production (Appel et al., 2008), respectively. NS5A DI purified from bacteria revealed two forms of dimers (PDB: 1ZH1, 3FQM) (Love et al., 2009; Tellinghuisen et al., 2005) (Figure 3A). These two forms of dimers were verified to exist *in vivo* by a mammalian two-hybrid system (Shanmugam et al., 2018). Based on the structures of these two dimers, we introduced TAG into residues W84 and K166, which are close to the interface of the 1ZH1-specific dimer but far from the interface of 3FQM-specific dimer, and into residues R48, E116, and F149, which are close to the interface of the 3FQM-specific dimer but far from the interface of 1ZH1-specific dimer. We also introduced TAG into residue A92 and T94, which are close to the interfaces of both dimers (Figure 3A). We proposed that the crosslink between the specific sites was associated with the presence of the specific dimer. After photocrosslinking, there was obvious crosslink at residue W84, resulting in a specific protein band with a molecular weight equivalent to that of the NS5A dimer (arrow, Figure 3B). Meanwhile, a faint crosslinked band at residue T94 was observed (Figures 3B and 3D). In contrast, no obvious crosslink at residues R48, E116, and F149 was observed (Figures 3C and 3D). These results suggest that the 1ZH1-specific dimer may exist as a preferred species *in vivo*.

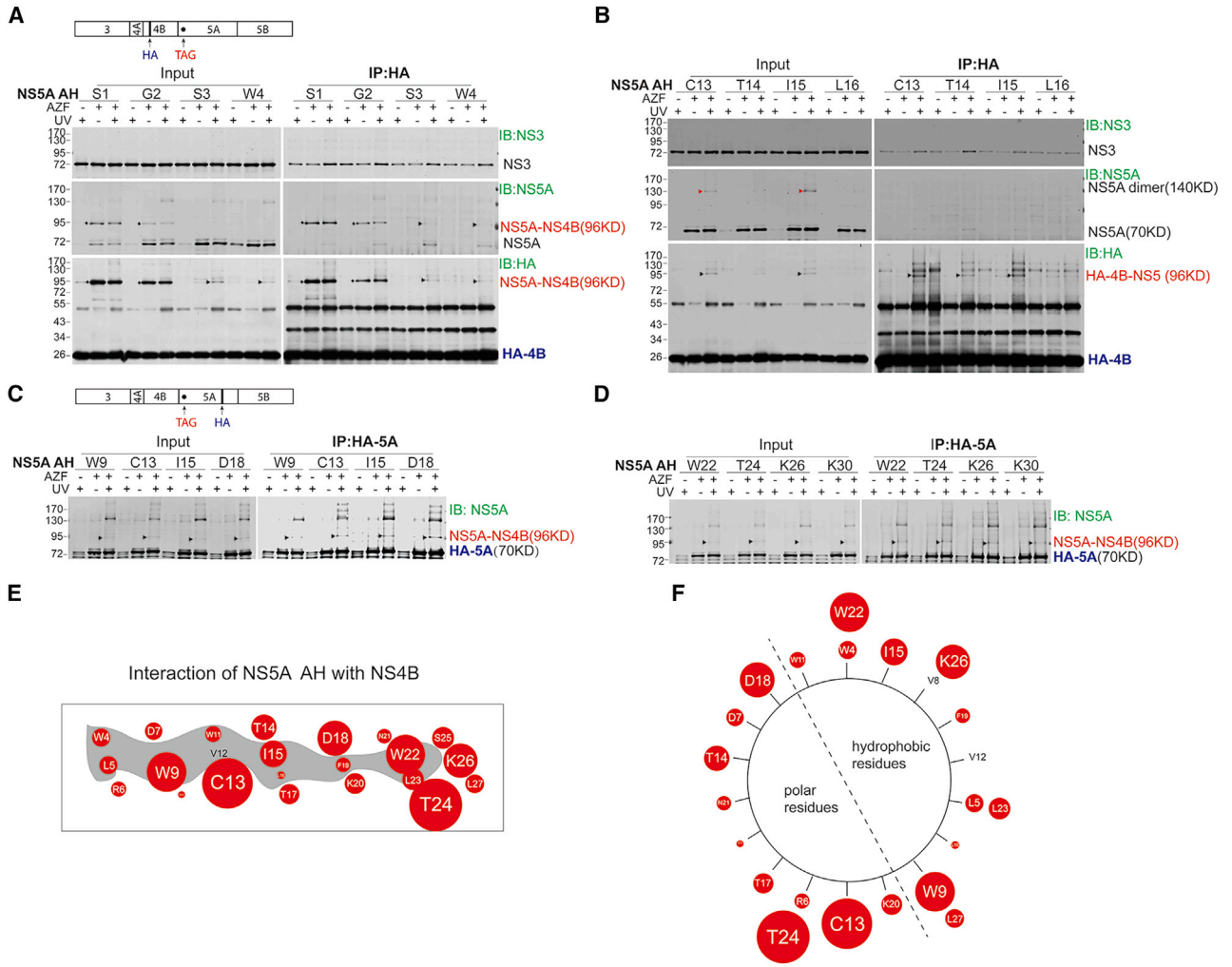

Figure 4. Identification of NS4B-interacting sites on the NS5A AH

(A and B) Photocrosslinking of NS5A AH mutants in the backbone of NS3-5B-4B^{HA}. TAG (red) was introduced in the NS5A AH regions at the indicated amino acids. Arrows indicate the crosslinked protein complexes. Squares indicate the unprocessed NS4B-NS5A. The expected molecular weight (kD) of the crosslinked protein complex is indicated. Red arrows in (B) indicate NS5A dimers.

(C and D) Photocrosslinking of NS5A AH mutants in the backbone of NS3-5B-5A^{HA}. TAG (red) was introduced in the NS5A AH regions at the indicated amino acids. Arrows indicate crosslinked protein complexes. The expected molecular weight (kD) of the crosslinked protein complex is indicated.

(E) Schematic representation of the NS5A AH-NS4B interaction. The amino acid sequence of NS5A AH from amino acids 4 to 27 is shown. The hydrophobic face of the helix is shaded in gray. The abundance of the NS5A-NS4B interaction complex was quantified, and the intensity of the NS5A AH-NS4B interaction was calculated by the ratio of the NS5A-NS4B complex after UV exposure to that before UV treatment and plotted as dots. The area of each dot represents the intensity of the NS5A AH and NS4B interaction at the indicated site.

(F) Schematic representation of the NS5A AH-NS4B interaction on the α-helical wheel.

To address the specificity of crosslinked band, we mutated the residues in the interface of the NS5A dimers as described previously (Shanmugam et al., 2018) and then examined W84-mediated photocrosslink. Mutations (F36A/I37A/S38A/R112A/E148A) that disrupt the interfaces of both NS5A dimers (Shanmugam et al., 2018) significantly diminished W84-mediated photocrosslink (arrows, Figures 3E and 3F), indicating that the crosslinked band corresponds to a specific NS5A dimer.

Identification of NS4B-interacting sites on the NS5A AH

We recently reported that NS5A AH regulates protein-protein interactions within the replicase components (Zhang et al., 2019a). Mutagenesis of NS5A AH and identification of suppressor mutations in the C terminus of NS4B indicate a genetic interaction of NS5A AH with NS4B (Biswas et al., 2016). To identify the NS4B-interacting residues on NS5A AH, we first introduced TAG into residues 1 through 30 of the NS5A AH in the backbone of NS3-5B.NS4B^{HA} (Figure 4A). The azF-NS5A AH variants were expressed, HA-NS4B was captured with anti-HA beads upon UV illumination, and the immunoprecipitated complexes were analyzed by SDS-PAGE and western blotting. As expected, incorporation of azF in resides S1 and G2 of NS5A AH obviously interrupted the processing at the junction of NS4B-NS5A, as shown by the reduction of the processed NS5A and the

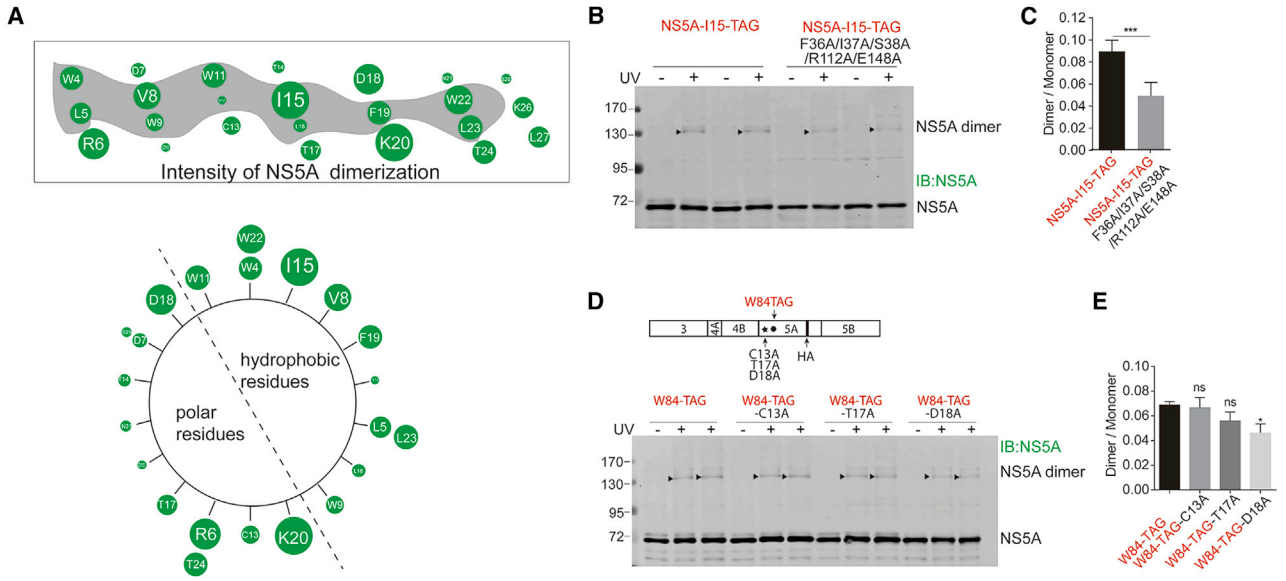

Figure 5. NS5A AH-mediated NS5A dimerization

(A) Schematic representation of NS5A dimerization. The amino acid sequence of NS5A AH is shown. The hydrophobic face of the helix is shaded in gray. The abundance of the NS5A dimer was quantified, and the intensity of NS5A dimerization was calculated by the ratio of the NS5A dimer to monomer and plotted as dots. The area of each dot represents the intensity of NS5A AH-mediated dimerization.

(B and C) Photocrosslinking of NS5A-I15-TAG mutants in the backbone of NS3-5B-5A^{HA}. A combination of mutations that disrupts the NS5A dimer interface was introduced in NS5A. Arrows indicate NS5A dimers. (C) The abundance of the NS5A dimer in (B) was quantified, and the ratio of the NS5A dimer to the NS5A monomer was calculated. Mean values ±SEM are shown (n = 5). Statistical analysis was performed between NS5A-I15-TAG and the NS5A AH mutant as indicated. ***$p < 0.001$, two-tailed, unpaired t test.

(D and E) Photocrosslinking of NS5A-W84-TAG mutants in the backbone of NS3-5B-5A^{HA}. Mutations were introduced in the NS5A AH. Arrows indicate NS5A dimers. (E) The abundance of the NS5A dimer in (D) was quantified, and the ratio of the NS5A dimer to the NS5A monomer was calculated. Mean values ± SDs are shown (n = 4). Statistical analysis was performed between NS5A-W84-TAG and the NS5A AH variants as indicated. *$p < 0.05$, two-tailed, unpaired t test.

presence of substantial amounts of NS4B-NS5A-specific species either before or after UV illumination in the anti-HA blot and the NS4B-NS5A counterparts in the anti-NS5A blot (squares, Figure 4A). UV-illumination-induced crosslinked products of equivalent size to unprocessed NS4B-NS5A were observed with azF variants at residues S3 and W4 (arrows, Figure 4A); L5, R6, and D7 (black arrows, Figure S7A); W9 and W11 (black arrows, Figure S7B); C13, T14, and I15 (black arrows, Figure 4B); T17, D18, F19, and K20 (black arrows, Figure S7C); N21, W22, L23, and T24 (black arrows, Figure S7D); S25, K26, L27, and F28 (black arrows, Figure S7E); and P29 and K30 (black arrows, Figure S7F) in the anti-HA-4B blot and the NS4B-NS5A counterparts in the anti-NS5A blot. Notably, the crosslinked NS4B-NS5A species were obscure in the anti-NS5A blot, probably due to the poor performance of the anti-NS5A antibody (Figures 4A and 4B). To better resolve NS4B-NS5A in the anti-NS5A blot, we further introduced TAGs into residues W9, C13, I15, D18, W22, T24, K26, and K30, which were identified to mediate strong NS4B-NS5A crosslink in the anti-HA-NS4B blot in the backbone of NS3-5B.NS5A^{HA} (Figures 4C and 4D). The azF-NS5A AH variants were expressed, and, upon UV illumination, the HA-NS5A-containing proteins were enriched by immunoprecipitation with anti-HA beads and then analyzed by SDS-PAGE and western blotting with antibodies against NS5A. UV-illumination-specific NS4B-NS5A complexes were unambiguously detected in all the variants (Figures 4C–4F; Table S1). Thus, we identified the NS4B-interacting sites on the NS5A N-terminal AH.

NS5A dimerization mediated by its AH

We noticed that there were crosslinked complexes with molecular weights equivalent to that of the NS5A dimer in the anti-NS5A blot in the series of azF-incorporated NS5A AH variants after photocrosslinking (red arrows in Figures 4B and S7), with various intensities for each residue (Figure 5A; Table S2), suggesting that NS5A dimerization occurs through the residues of the AH. We then explored the effect of NS5A domain I-mediated dimerization on NS5A dimerization mediated by the AH. We selected residue I15 in the AH, introduced the TAG in this residue, and disrupted domain I-mediated dimerization by mutating the dimer interface to examine the effect on NS5A dimerization via AH by evaluating the photocrosslink of residue I15. Mutation at the interface (F36A/I37A/S38A/R112A/E148A) of the domain I-mediated dimerization did not abolish but significantly reduced NS5A dimerization via residue I15 to 55% of the control level (Figures 5B and 5C). Next, we mutated residues that mediate dimerization in the AH region and examined the effect on domain I-mediated dimerization by evaluating the photocrosslink of residue W84 in domain I. We selected residues C13, T17, and D18 at the hydrophilic face of AH (Figure 5A) and mutated them to alanine in the NS3-5B-5A^{HA}-NS5A-W84-TAG backbone (Figure 5D). We evaluated the photocrosslink of residue W84 and observed that mutations of C13A and T17A did not affect NS5A dimerization. In contrast, mutation of D18A significantly reduced NS5A dimerization of residue W84 to 66% of the control level (Figures 5D and 5E).

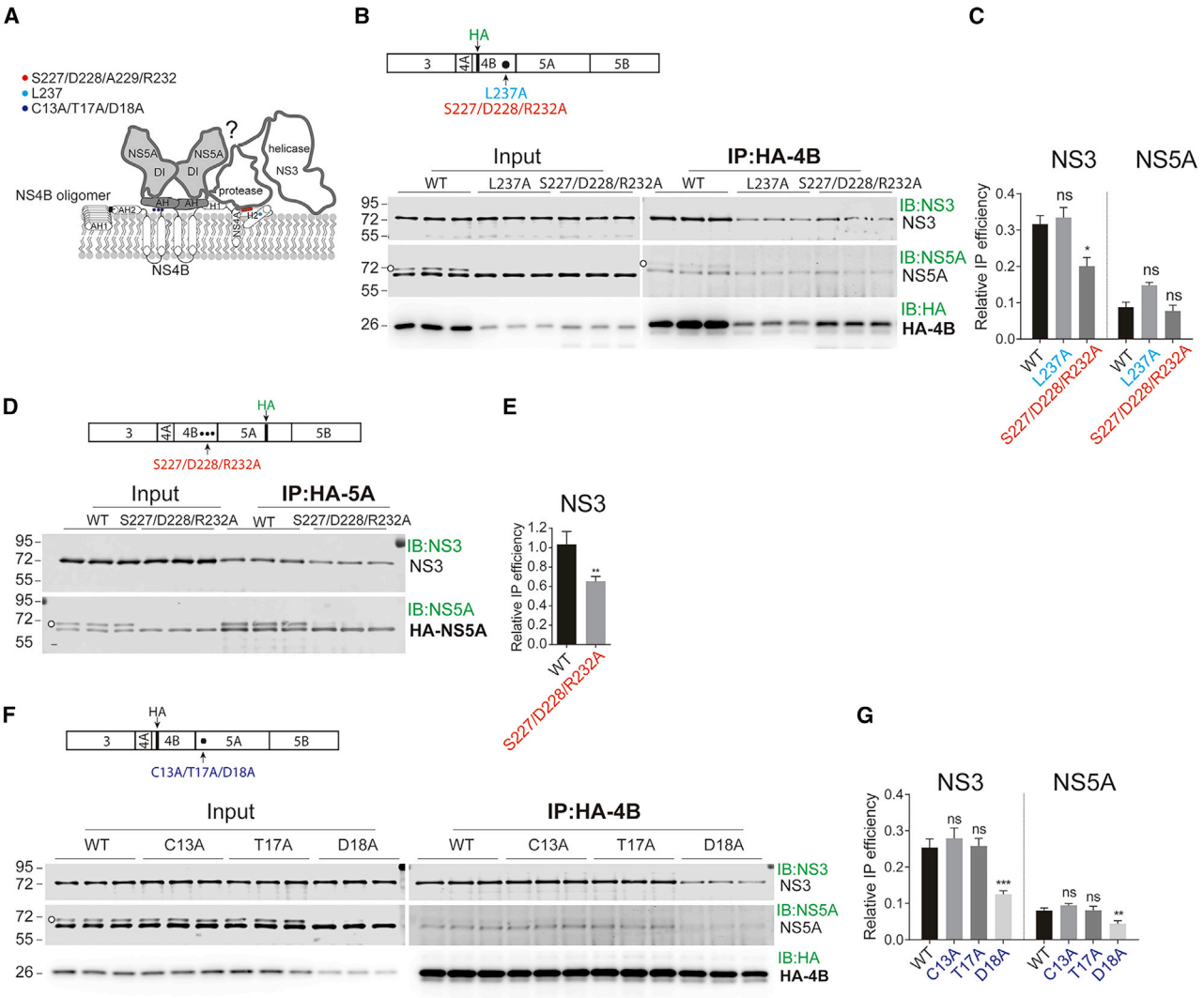

Figure 6. Docking sites of NS5A and NS3 on NS4B regulates interactions among NS3, NS5A, and NS4B

(A) Proposed model of HCV replicase. The NS4B oligomerization site (L237) on its H2 region (blue), NS3-interacting sites (S227/D228/R232) (red), and NS4B-interacting sites (D18) (purple) on NS5A AH are shown.

(B and C) Interaction of NS4B mutants with NS3 and NS5A in the context of NS3-5B-4B^{HA}. NS3-docking sites on NS4B were mutated as indicated. (B) HEK293T cells were transfected with HCV NS3-5B-4B^{HA} (WT) and indicated NS4B mutants. Cells were lysed, and the cell lysates were captured by anti-HA beads (IP). The captured proteins were analyzed by western blotting. Circles, hyperphosphorylated NS5A. (C) The relative IP efficiency in (B) was calculated as immunoprecipitated NS3 or NS5A/captured NS4B^{HA}. Mean values ± SEMs are shown (n = 6). Statistical analysis was performed between WT and the variants as indicated. *p < 0.05, two-tailed, unpaired t test.

(D and E) Interaction of NS3 with NS5A when the NS3-docking sites on NS4B were mutated in the context of NS3-5B-5A^{HA}. Circle, hyperphosphorylated NS5A. (E) The relative IP efficiency in (D) was calculated as immunoprecipitated NS3/captured NS5A^{HA}. Mean values ± SDs are shown (n = 3). Statistical analysis was performed between WT and the variant as indicated. **p < 0.01, two-tailed, unpaired t test.

(F and G) Interaction of NS4B with NS3 and NS5A when the NS4B-docking sites on NS5A were mutated in the context of NS3-5B-4B^{HA}. Circle, hyperphosphorylated NS5A. (G) The relative IP efficiency in (F) was calculated as immunoprecipitated NS3 or NS5A/captured NS4B^{HA}. Mean values ± SEMs are shown (n = 6). Statistical analysis was performed between WT and the indicated variants. **p < 0.01, ***p < 0.001; two-tailed, unpaired t test.

These results indicate the N-terminal AH and domain I reciprocally regulate NS5A dimerization.

Docking of NS5A and NS3 on NS4B regulates protein-protein interactions among the replicase components

Based on the photocrosslinking results, NS3 interacted with NS4B via the residues in the C-terminal region of NS4B (Figures 2 and 6A) and resides in the NS5A AH participated in the NS5A-NS4B interaction (Table S1 and Figure 6A). We hypothesized that docking of NS5A and NS3 on NS4B regulates protein-protein interactions among the replicase components. First, we mutated the docking sites of NS3 on NS4B and then examined the effects on the NS3-NS5A interaction. We verified the effect of the mutations on the NS4B-NS3 interaction by a coimmunoprecipitation experiment. We introduced a mutation combination (S227A/D228A/R232A) of NS3 docking sites and the L237A mutation

that disrupts NS4B oligomerization (Figure 1F) into the NS3-5B-4B^{HA} backbone and then captured the HA-NS4B-associated complexes by anti-HA magnetic beads. As expected, mutation of the NS3 docking sites on NS4B significantly reduced the NS4B-NS3 interaction but did not affect the NS4B-NS5A interaction (Figures 6B and 6C). Disruption of NS4B oligomerization by the L237A mutation affected neither the NS4B-NS3 nor NS4B-NS5A interaction (Figures 6B and 6C). Then, we examined the mutation of the NS3 docking sites on NS4B in the NS5A-NS3 interaction. We introduced these mutants into the NS3-5B-5A^{HA} backbone and captured the HA-NS5A-associated complex by anti-HA magnetic beads. Mutation of the NS3 docking sites significantly reduced the NS5A-NS3 interaction (Figures 6D and 6E), indicating that the NS3-NS4B interaction affects the NS5A-NS3 interaction. Notably, the NS4B mutations affected the hyperphosphorylation of NS5A and the expression level of NS4B (Figure 6B).

We also examined the impact of the interaction of the NS5A AH with NS4B on the NS4B-NS3 interaction. We selected residues C13, T17, and D18 in the NS5A AH, where photocrosslinking with NS4B occurred (Figures 4E and 4F), and introduced mutations into the NS3-5B-4B^{HA} backbone. The HA-NS4B-associated complex was captured and analyzed as described above. Mutations C13A and T17A did not affect the NS5A-NS4B interaction, probably due to the interactions compensated for by other residues. Mutation D18A significantly reduced the NS5A-NS4B interaction (Figures 6F and 6G). Strikingly, it also significantly reduced the NS4B-NS3 interaction, indicating that the NS5A-NS4B interaction affects the NS4B-NS3 interaction (Figures 6F and 6G). Notably, the D18A but not the NS4B C13A and T17A mutations affected the hyperphosphorylation of NS5A (Figure 6F). Taken together, these data indicate that the NS3-NS4B and NS5A-NS4B interactions affected the protein-protein interactions among the replicase components (see discussion).

Disruption of the interactome of the hepatitis C virus replicase abolished HCV replication

Finally, we assessed the impact of the identified interactome on viral replication. We used the subgenomic replicon sgJFH1-sGluc expressing secreted Gaussia luciferase (sGluc) (Zhang et al., 2019a), introduced point mutations into sgJFH1-sGluc, and then assessed viral replication by monitoring the luciferase activity (Figure 7A). Several residues involved in the interactome have been reported to affect viral replication in previous studies (Biswas et al., 2016; Elazar et al., 2004; Gouttenoire et al., 2014) (Figure 7B). The results showed that mutation of NS4B.L237A (which impairs NS4B oligomerization), NS5A.W84A (in the NS5A interface) and NS4B.D228A (which mediates the NS4B-NS3 interaction) abolished viral replication (Figures 7A and 7B). NS4B.S227A mutation attenuated viral replication, whereas NS4B.S232A mutation did not affect viral replication (Figures 7A and 7B).

DISCUSSION

In this study, we used a viral replicase assembly surrogate system wherein the HCV NS3-5B polyprotein is expressed to mimic the induction of the viral replicase for several reasons. First, this method segregates the replicase assembly from viral replication, which makes it possible to perform mutagenesis of the replicase component. Second, the expression of the NS3-5B polyprotein induces the formation of the viral RC as in HCV-infected cells (Romero-Brey et al., 2012). Third, the HCV NS5A inhibitors prevent the formation of RC (Berger et al., 2014) and impair protein-protein interactions (Zhang et al., 2019b) in this surrogate system. Fourth, the expression of NS3-5B can *trans*-complement lethal mutations in the replicase components (Kazakov et al., 2015). These findings indicate that interactions among the replicase components or with host factors in the surrogate system recapitulate the scenario in virally infected cells.

NS4B oligomerization

Previous studies reported that NS4B oligomerized mainly through the N-terminal AH2 and C-terminal H1 by using a means of FRET (Gouttenoire et al., 2010b; Paul et al., 2011). However, the self-interacting sites or contacting sites in the NS4B oligomer and the oligomerization pattern remain determined. By using photocrosslinking, we detected robust crosslinked NS4B oligomers through residues in the N-terminal AH1 and residues in the linker regions between AH1 and AH2 (Figure 1H), as well as through residue L237 in the C-terminal H2 region (Figure 1H), indicating that these residues are contacting residues in the NS4B oligomers. Importantly, mutation of L237 impaired NS4B dimerization and oligomerization (Figure 1F), indicating that residue L237 is required for NS4B dimerization and oligomerization. In a previous study, mutation of L237 and L240 to L237AL240A only slightly affected membrane association of NS4B determined by membrane flotation and resulted in much smaller dot-like structures under immunofluorescence microscopy without affecting the NS4B-NS5A colocalization (Gouttenoire et al., 2009). Given the findings here, these smaller dot-like structures might be due to the impairment of NS4B oligomerization. We could not detect crosslinking at the residues in N-terminal AH2 and C-terminal H1, probably because these residues are important for initiating NS4B oligomerization (Gouttenoire et al., 2010b; Paul et al., 2011) and replacement of these residues with azF impairs NS4B oligomerization. We readily detected the dimer, tetramer, hexamer, and octamer but not the trimer of NS4B (Figure 1C). NS4B trimer has been detected by using glutaraldehyde-mediated crosslinking (Yu et al., 2006), probably due to the insufficient specificity of chemical agent-mediated crosslinking. Even though we could not unambiguously determine the bigger oligomers than octamer due to the detection limit of SDS-PAGE, we could imagine that NS4B dimerization is initiated probably through residues in N-terminal AH2 and C-terminal H1 (Gouttenoire et al., 2010b; Paul et al., 2011); the dimeric NS4B then interacts homotypically (side by side via same region) and heterotypically (head to tail via different regions) through the residues in the N-terminal contacting sites and the residue L237 in the C-terminal H2 region (Figure 1) to form NS4B oligomers (Figure 7C).

NS4B acts as a platform for replicase assembly

The capability of NS4B to oligomerize makes it a candidate platform for replicase assembly. Genetic complement experiments demonstrate interactions between the NS4B C-terminal element with NS5A domain I (Paul et al., 2011) and the NS5A AH (Biswas

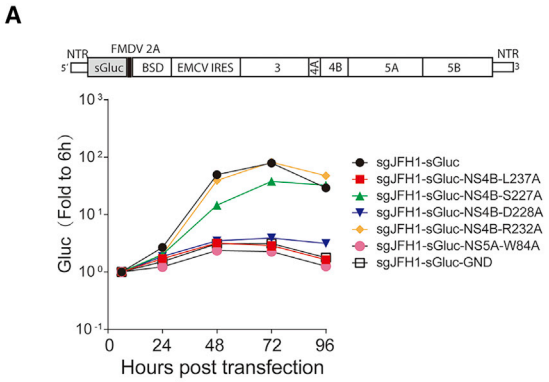

B

Summary of the impact of the mutants on viral replication

Phenotypes	Mutation	Replication	Reference
(Nonstructural Protein)			
NS4B oligomerization (**NS4B**)	K18A	-	(Gouttenoire et al., 2014)
	K20A	-	(Gouttenoire et al., 2014)
	K18A/K20A	-	(Gouttenoire et al., 2014)
	G10E	-	(Elazar et al., 2004)
	A21E	-	(Elazar et al., 2004)
	L24E	-	(Elazar et al., 2004)
	L237A	-	This study
NS5A dimerization (**NS5A**)	W84A	-	This study
NS4B-NS5A interaction (**NS5A**)	D7K/D10K	-	(Biswas et al., 2016)
	C13E	-	(Biswas et al., 2016)
	T17L	-	(Biswas et al., 2016)
	D18K	-	(Biswas et al., 2016)
	K20D	-	(Biswas et al., 2016)
NS4B-NS3 interaction (**NS4B**)	S227A	-/+	This study
	D228A	-	This study
	R232A	+	This study

+, same as the wild type; -, abolished replication; +/-, attenuated replication

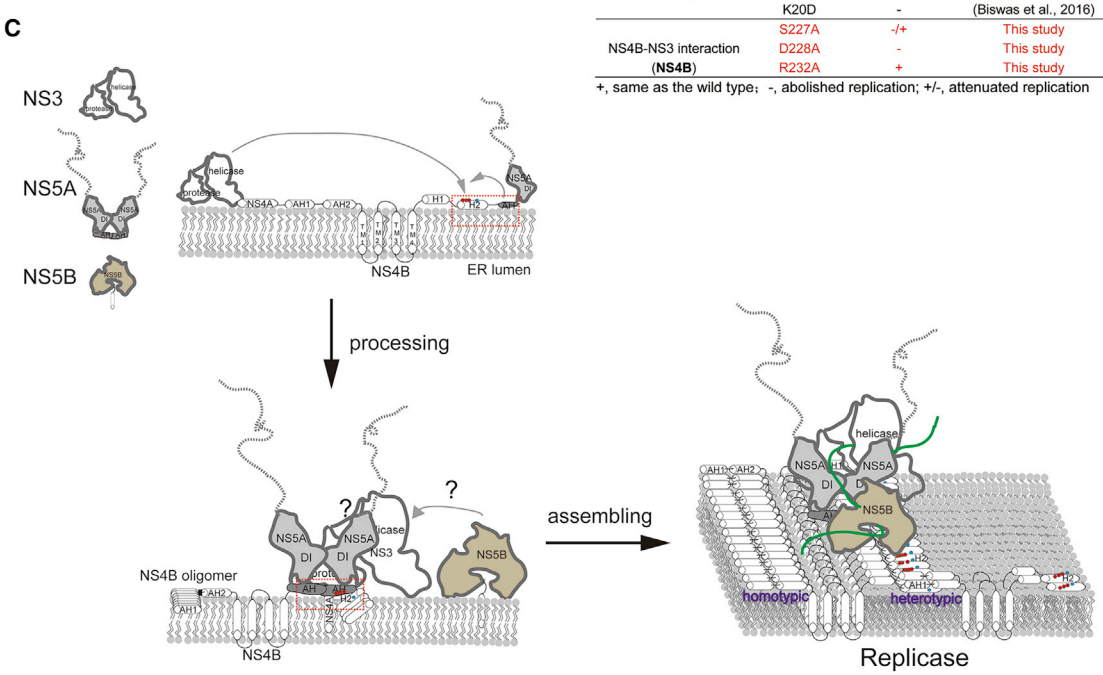

Figure 7. Disruption of the interactions among the replicase components abolishes HCV replication

(A) Replicon RNAs sgJFH1-sGluc and variants bearing the indicated mutations were transfected into Huh7.5 cells in triplicate wells. Luciferase activity in the supernatants was measured and plotted. Mean values ± SDs are shown (n = 3).

(B) Summary of the impact of the mutants on viral replication.

(C) The model of HCV replicase assembly. The models of the proteins may not reflect their real sizes. The NS3-NS5A interacting sites and the NS3-NS5B interacting sites are unknown. The red dashed box indicates the hub element for replicase assembly. In the proposed replicase model, viral RNA is green. See details in the main text.

et al., 2016). The NS4B-NS5A interaction is required for proper NS5A localization (Biswas et al., 2016). In this study, we identified the docking sites of NS3 on NS4B in the C-terminal α-helix H2 of NS4B (Figure 2). Combination mutations of these docking sites significantly reduced the NS3-NS4B interaction (Figures 6B and 6C). By photocrosslinking, we also detected the NS4B-NS5A interaction mediated by the NS5A AH (Figure 4). Unfortunately, we could not reciprocally identify the docking sites of NS5A on NS4B by using the NS4B-azF variants. One of the reasons is the poor performance of the anti-NS5A antibodies. Given the observations that some of the residues mediating NS5A dimerization in the NS5A AH (Figure 5A) overlapped with some of the residues that mediate the NS5A AH-NS4B interaction (Figures 4E and 4F), it is possible that the oligomerization sites of NS4B may somehow overlap with the NS5A docking sites, which makes it difficult to unambiguously identify the NS5A-interacting sites.

NS5A dimerization

Two forms of dimeric NS5A domain I (PDB: 1ZH1, 3FQM) have been reported (Love et al., 2009; Tellinghuisen et al., 2005). Experiments using a mammalian two-hybrid system have indicated the existence of both forms *in vivo* (Shanmugam et al., 2018). In this study, we only detected obvious 1ZH1-specific dimer in cells (Figure 3). We failed to detect a 3FQM-specific dimer, probably due to its relatively low abundance. In addition to the

domain I-mediated NS5A dimer, we identified dimerization of NS5A through the N-terminal AH (Figure 5A). Disruption of domain I-mediated dimerization impaired AH-mediated dimerization and vice versa (Figures 5B–5E), indicating that AH-mediated dimerization reciprocally prompts domain I-mediated dimerization.

A positively charged groove that is proposed to participate in RNA binding exists only in the 1ZH1-specific dimer (Tellinghuisen et al., 2005) (Figure 7C). Biochemical evidence has shown NS5A to be an RNA-binding protein with a preference for single-stranded RNA (Huang et al., 2005). Pharmacological inhibitors of NS5A and NS5A-interacting host factor VCP imply the existence of polymers of NS5A within the cells (Sun et al., 2015; Yi and Yuan, 2017). Our photocrosslinking experiment only detected dimeric NS5A (Figures 3 and 5). We cannot exclude the possibility that, in the presence of viral RNA, multiple dimeric NS5As bind to viral RNA to form multimers (Figure 7C). In an *in vitro* replication system that uses an artifact rolling-circle RNA as a template, NS5A has been demonstrated to be a processivity factor for viral RNA synthesis (Mani et al., 2015), which is probably attributed to the binding of viral RNA by dimeric NS5A (Figure 7C).

The C-terminal α-helix H2 of NS4B and the NS5A AH are hub elements for replicase assembly

Mutating the docking sites of NS3 on the C-terminal α-helix H2 of NS4B significantly reduced the NS5A-NS3 interaction (Figures 6D and 6E), indicating that docking of NS3 on NS4B facilitates the NS3-NS5A interaction. Reciprocally, the NS5A AH mutation D18A, which impaired the NS5A-NS4B interaction (Figures 6F and 6G), significantly reduced the NS4B-NS3 interaction (Figures 6F and 6G). These data indicate a scenario in which the interaction of NS5A and NS3 with NS4B facilitates the reciprocal interaction between NS3 and NS5A to form a protein complex containing NS4B, NS3, and NS5A, although the interacting interface of NS3-NS5A remains to be identified (Figure 7C). Notably, disruption of NS4B oligomerization by the L237A mutation in the C-terminal α-helix H2 of NS4B affected neither the NS4B-NS3 nor NS4B-NS5A interaction (Figures 6B and 6C), indicating that NS4B oligomerization is not required for the NS4B-mediated NS3-NS5A interaction. However, mutation of the NS3 docking sites (D228) and the oligomerization sites (L237) of the C-terminal α-helix H2 of NS4B abolished viral replication (Figures 7A and 7B), pointing to the critical role of C-terminal α-helix H2 of NS4B in replicase assembly. We recently reported that the NS5A AH regulates polyprotein processing and protein-protein interactions within the replicase (Zhang et al., 2019a). In this study, we identified the NS5A AH-mediated NS5A-NS4B interaction, and mutations of the residues that participate in the interaction have been reported to abolish viral replication (Figure 7B) (Biswas et al., 2016). These data suggest the C-terminal α-helix H2 of NS4B and the NS5A AH function as hub elements in replicase assembly by mediating NS4B oligomerization and recruiting NS3 and NS5A to prompt the NS3-NS4B-NS5A interaction (red box, Figure 7C).

Due to the unavailability of an anti-NS5B antibody, we could not map the interactome involving NS5B. The NS3 helicase domain has been reported to interact directly with NS5B to form a stable complex in an *in vitro* replication system (Mani et al., 2015). GST pull-down experiment revealed interactions between the NS3 protease domain and NS5B (Zhang et al., 2005). It has been demonstrated in a replicase assembly surrogate system similar to the one used in this study that the HCV NS3 helicase domain is required for viral RC assembly (Romero-Brey et al., 2015). In a previous study, we detected the NS5B-NS3 and NS5B-NS5A interactions in a similar replicase assembly surrogate system by coimmunoprecipitation (Zhang et al., 2019b). It is possible that NS5B is recruited to the NS3-NS4B-NS5A complex via interaction with NS3 to assemble the fully formed replicase (Figure 7C). Biochemical studies *in vitro* have suggested that NS5B lacks template specificity, has poor affinity for HCV RNA (Behrens et al., 1996; Lohmann et al., 1997, 1998), and has inefficient catalytic activity in the absence of other viral proteins (Lohmann et al., 1998; Mani et al., 2015; Tomei et al., 2000). We proposed that, *in vivo*, the protein-protein interactions within the replicase components and the interactions between the replicase components and the viral RNA template ensure that the viral RNA polymerase precisely accommodates the viral RNA template for *de novo* RNA synthesis (Figure 7C). The HCV RNA helicase domain in NS3 employs a "ratchet" mechanism for unidirectional translocation of the template (Gu and Rice, 2010). Although the exact role of HCV NS3 helicase activity in the replicase is still unclear, it might trigger movement of the viral RNA template during viral replication, which is analogous to the helicase of brome mosaic virus protein 1a in recruiting the viral template (Ahola et al., 2000).

In summary, by using a bioorthogonal strategy, we dissected the interactome of the HCV replicase and identified key elements that are important for replicase assembly. These findings advance our knowledge about the replicase assembly in positive-strand RNA viruses. The strategy used here may be employed to dissect the replicase assembly of other positive-strand RNA viruses, which may inspire the development of antiviral agents against these viruses.

SIGNIFICANCE

Assembly of viral replicase on host membranes is a conserved replication strategy and an attractive antiviral target for positive-strand RNA viruses. Studies on multiprotein complexes involved in replication of positive-strand RNA viruses are technically challenging. In this study, we employ a bioorthogonal method to dissect the replicase assemble of HCV. Our results generate a detailed landscape of protein-protein interactions and reveal hub elements in replicase assembly. Our findings provide insights into the underlying molecular mechanism of viral replicase assembly and may inspire the studies of other positive-strand RNA viruses for development of direct antiviral agents.

STAR★METHODS

Detailed methods are provided in the online version of this paper and include the following:

- KEY RESOURCES TABLE
- RESOURCE AVAILABILITY
  - Lead contact
- MATERIALS AVAILABILITY

SUPPLEMENTAL INFORMATION

Supplemental information can be found online at https://doi.org/10.1016/j.chembiol.2021.03.006.

ACKNOWLEDGMENTS

We are grateful to Charles Rice (Rockefeller University) and Thomas P. Sakmar (Rockefeller University) for kindly sharing the research reagents, and to Margaret R. MacDonald (The Rockefeller University) for her critical reading of the manuscript and enlightening discussion. This work was supported in part by the National Natural Science Foundation of China (81971926 and 81772181 to Z.-G.Y.) and the National Science and Technology Major Project of China (2017ZX10103009 to Z.-G.Y.). This study is dedicated to our mentor Yumei Wen on the occasion of her 87th birthday. She started teaching and working on medical virology about 50 years ago and is still active. She popularized scientific knowledge about the SARS-CoV-2 to the public and encouraged us to devote ourselves to the scientific struggle against the COVID-19 pandemic.

AUTHOR CONTRIBUTIONS

Conceptualization, Z.-G.Y.; investigation, Y.Z. and S.C.; data analysis, Z.-G.Y. and Y.Z.; writing original draft, Z.-G.Y. and Y.Z.; editing, Z.-H.Y.; resources, Z.-H.Y. and Z.-G.Y.

DECLARATION OF INTERESTS

The authors declare no competing interests.

Received: January 16, 2021
Revised: February 21, 2021
Accepted: March 10, 2021
Published: April 1, 2021

REFERENCES

Ahola, T., den Boon, J.A., and Ahlquist, P. (2000). Helicase and capping enzyme active site mutations in brome mosaic virus protein 1a cause defects in template recruitment, negative-strand RNA synthesis, and viral RNA capping. J. Virol. *74*, 8803–8811.

Appel, N., Zayas, M., Miller, S., Krijnse-Locker, J., Schaller, T., Friebe, P., Kallis, S., Engel, U., and Bartenschlager, R. (2008). Essential role of domain III of nonstructural protein 5A for hepatitis C virus infectious particle assembly. PLoS Pathog. *4*, e1000035.

Behrens, S.E., Tomei, L., and De Francesco, R. (1996). Identification and properties of the RNA-dependent RNA polymerase of hepatitis C virus. EMBO J. *15*, 12–22.

Berger, C., Romero-Brey, I., Radujkovic, D., Terreux, R., Zayas, M., Paul, D., Harak, C., Hoppe, S., Gao, M., Penin, F., et al. (2014). Daclatasvir-like inhibitors of NS5A block early biogenesis of hepatitis C virus-induced membranous replication factories, independent of RNA replication. Gastroenterology *147*, 1094–1105.e25.

Biswas, A., Treadaway, J., and Tellinghuisen, T.L. (2016). Interaction between nonstructural proteins NS4B and NS5A is essential for proper NS5A localization and hepatitis C virus RNA replication. J. Virol. *90*, 7205–7218.

Chung, H.Y., Gu, M., Buehler, E., MacDonald, M.R., and Rice, C.M. (2014). Seed sequence-matched controls reveal limitations of small interfering RNA knockdown in functional and structural studies of hepatitis C virus NS5A-MOBKL1B interaction. J. Virol. *88*, 11022–11033.

den Boon, J.A., and Ahlquist, P. (2010). Organelle-like membrane compartmentalization of positive-strand RNA virus replication factories. Annu. Rev. Microbiol. *64*, 241–256.

Dujardin, M., Madan, V., Montserret, R., Ahuja, P., Huvent, I., Launay, H., Leroy, A., Bartenschlager, R., Penin, F., Lippens, G., et al. (2015). A proline-tryptophan turn in the intrinsically disordered domain 2 of NS5A protein is essential for hepatitis C virus RNA replication. J. Biol. Chem. *290*, 19104–19120.

Egger, D., Wolk, B., Gosert, R., Bianchi, L., Blum, H.E., Moradpour, D., and Bienz, K. (2002). Expression of hepatitis C virus proteins induces distinct membrane alterations including a candidate viral replication complex. J. Virol. *76*, 5974–5984.

Elazar, M., Liu, P., Rice, C.M., and Glenn, J.S. (2004). An N-terminal amphipathic helix in hepatitis C virus (HCV) NS4B mediates membrane association, correct localization of replication complex proteins, and HCV RNA replication. J. Virol. *78*, 11393–11400.

Gao, M., Nettles, R.E., Belema, M., Snyder, L.B., Nguyen, V.N., Fridell, R.A., Serrano-Wu, M.H., Langley, D.R., Sun, J.H., O'Boyle, D.R., 2nd, et al. (2010). Chemical genetics strategy identifies an HCV NS5A inhibitor with a potent clinical effect. Nature *465*, 96–100.

Gouttenoire, J., Montserret, R., Kennel, A., Penin, F., and Moradpour, D. (2009). An amphipathic alpha-helix at the C terminus of hepatitis C virus nonstructural protein 4B mediates membrane association. J. Virol. *83*, 11378–11384.

Gouttenoire, J., Montserret, R., Paul, D., Castillo, R., Meister, S., Bartenschlager, R., Penin, F., and Moradpour, D. (2014). Aminoterminal amphipathic alpha-helix AH1 of hepatitis C virus nonstructural protein 4B possesses a dual role in RNA replication and virus production. PLoS Pathog. *10*, e1004501.

Gouttenoire, J., Penin, F., and Moradpour, D. (2010a). Hepatitis C virus nonstructural protein 4B a journey into unexplored territory. Rev. Med. Virol. *20*, 117–129.

Gouttenoire, J., Roingeard, P., Penin, F., and Moradpour, D. (2010b). Amphipathic alpha-helix AH2 is a major determinant for the oligomerization of hepatitis C virus nonstructural protein 4B. J. Virol. *84*, 12529–12537.

Gu, M., and Rice, C.M. (2013). Structures of hepatitis C virus nonstructural proteins required for replicase assembly and function. Curr. Opin. Virol. *3*, 129–136.

Gu, M.G., and Rice, C.M. (2010). Three conformational snapshots of the hepatitis C virus NS3 helicase reveal a ratchet translocation mechanism. Proc. Natl. Acad. Sci. U S A *107*, 521–528.

Huang, L.Y., Hwang, J., Sharma, S.D., Hargittai, M.R.S., Chen, Y.F., Arnold, J.J., Raney, K.D., and Cameron, C.E. (2005). Hepatitis C virus nonstructural protein 5A (NS5A) is an RNA-binding protein. J. Biol. Chem. *280*, 36417–36428.

Huber, T., and Sakmar, T.P. (2014). Chemical biology methods for investigating G protein-coupled receptor signaling. Chem. Biol. *21*, 1224–1237.

Kazakov, T., Yang, F., Ramanathan, H.N., Kohlway, A., Diamond, M.S., and Lindenbach, B.D. (2015). Hepatitis C virus RNA replication depends on specific cis- and trans-acting activities of viral nonstructural proteins. PLoS Pathog. *11*, e1004817.

Kohli, A., Shaffer, A., Sherman, A., and Kottilil, S. (2014). Treatment of hepatitis C: a systematic review. JAMA *312*, 631–640.

Lohmann, V., Korner, F., Herian, U., and Bartenschlager, R. (1997). Biochemical properties of hepatitis C virus NS5B RNA-dependent RNA

polymerase and identification of amino acid sequence motifs essential for enzymatic activity. J. Virol. *71*, 8416–8428.

Lohmann, V., Roos, A., Korner, F., Koch, J.O., and Bartenschlager, R. (1998). Biochemical and kinetic analyses of NS5B RNA-dependent RNA polymerase of the hepatitis C virus. Virology *249*, 108–118.

Love, R.A., Brodsky, O., Hickey, M.J., Wells, P.A., and Cronin, C.N. (2009). Crystal structure of a novel dimeric form of NS5A domain I protein from hepatitis C virus. J. Virol. *83*, 4395–4403.

Lundin, M., Lindstrom, H., Gronwall, C., and Persson, M.A.A. (2006). Dual topology of the processed hepatitis C virus protein NS4B is influenced by the NS5A protein. J. Gen. Virol. *87*, 3263–3272.

Mani, N., Yuzhakov, A., Yuzhakov, O., Coll, J.T., Black, J., Saxena, K., Fulghum, J.R., Lippke, J.A., Rao, B.G., Rijnbrand, R., et al. (2015). Nonstructural protein 5A (NS5A) and human replication protein A increase the processivity of hepatitis C virus NS5B polymerase activity in vitro. J. Virol. *89*, 165–180.

Manns, M.P., Buti, M., Gane, E., Pawlotsky, J.M., Razavi, H., Terrault, N., and Younossi, Z. (2017). Hepatitis C virus infection. Nat. Rev. Dis. Primers *3*, 17006.

Moradpour, D., Penin, F., and Rice, C.M. (2007). Replication of hepatitis C virus. Nat. Rev. Microbiol. *5*, 453–463.

Naganathan, S., Grunbeck, A., Tian, H., Huber, T., and Sakmar, T.P. (2013). Genetically-encoded molecular probes to study G protein-coupled receptors. J. Vis. Exp. *79*, 50588.

Paul, D., Hoppe, S., Saher, G., Krijnse-Locker, J., and Bartenschlager, R. (2013). Morphological and biochemical characterization of the membranous hepatitis C virus replication compartment. J. Virol. *87*, 10612–10627.

Paul, D., Romero-Brey, I., Gouttenoire, J., Stoitsova, S., Krijnse-Locker, J., Moradpour, D., and Bartenschlager, R. (2011). NS4B self-interaction through conserved C-terminal elements is required for the establishment of functional hepatitis C virus replication complexes. J. Virol. *85*, 6963–6976.

Petersen, L.R., Jamieson, D.J., Powers, A.M., and Honein, M.A. (2016). Zika virus. N. Engl. J. Med. *374*, 1552–1563.

Romero-Brey, I., Berger, C., Kallis, S., Kolovou, A., Paul, D., Lohmann, V., and Bartenschlager, R. (2015). NS5A domain 1 and polyprotein cleavage kinetics are critical for induction of double-membrane vesicles associated with hepatitis C virus replication. mBio *6*, e00759.

Romero-Brey, I., Merz, A., Chiramel, A., Lee, J.Y., Chlanda, P., Haselman, U., Santarella-Mellwig, R., Habermann, A., Hoppe, S., Kallis, S., et al. (2012). Three-dimensional architecture and biogenesis of membrane structures associated with hepatitis C virus replication. PLoS Pathog. *8*, e1003056.

Ross-Thriepland, D., Amako, Y., and Harris, M. (2013). The C terminus of NS5A domain II is a key determinant of hepatitis C virus genome replication, but is not required for virion assembly and release. J. Gen. Virol. *94*, 1009–1018.

Sato, S., Mimasu, S., Sato, A., Hino, N., Sakamoto, K., Umehara, T., and Yokoyama, S. (2011). Crystallographic study of a site-specifically cross-linked protein complex with a genetically incorporated photoreactive amino acid. Biochemistry *50*, 250–257.

Shanmugam, S., Nichols, A.K., Saravanabalaji, D., Welsch, C., and Yi, M.K. (2018). HCV NS5A dimer interface residues regulate HCV replication by controlling its self-interaction, hyperphosphorylation, subcellular localization and interaction with cyclophilin A. PLoS Pathog. *14*, e1007177.

Sun, J.H., O'Boyle, D.R., Fridell, R.A., Langley, D.R., Wang, C.F., Roberts, S.B., Nower, P., Johnson, B.M., Moulin, F., Nophsker, M.J., et al. (2015). Resensitizing daclatasvir-resistant hepatitis C variants by allosteric modulation of NS5A. Nature *527*, 245–248.

Tellinghuisen, T.L., Marcotrigiano, J., and Rice, C.M. (2005). Structure of the zinc-binding domain of an essential component of the hepatitis C virus replicase. Nature *435*, 374–379.

Tomei, L., Vitale, R.L., Incitti, I., Serafini, S., Altamura, S., Vitelli, A., and De Francesco, R. (2000). Biochemical characterization of a hepatitis C virus RNA-dependent RNA polymerase mutant lacking the C-terminal hydrophobic sequence. J. Gen. Virol. *81*, 759–767.

Unchwaniwala, N., Zhan, H., Pennington, J., Horswill, M., den Boon, J.A., and Ahlquist, P. (2020). Subdomain cryo-EM structure of nodaviral replication protein A crown complex provides mechanistic insights into RNA genome replication. Proc. Natl. Acad. Sci. U S A *117*, 18680–18691.

Ye, S.X., Kohrer, C., Huber, T., Kazmi, M., Sachdev, P., Yan, E.C.Y., Bhagat, A., RajBhandary, U.L., and Sakmar, T.P. (2008). Site-specific incorporation of keto amino acids into functional G protein-coupled receptors using unnatural amino acid mutagenesis. J. Biol. Chem. *283*, 1525–1533.

Yi, Z., Fang, C., Zou, J., Xu, J., Song, W., Du, X., Pan, T., Lu, H., and Yuan, Z. (2016). Affinity purification of the hepatitis C virus replicase identifies valosin-containing protein, a member of the ATPases associated with diverse cellular activities family, as an active virus replication modulator. J. Virol. *90*, 9953–9966.

Yi, Z.G., and Yuan, Z.H. (2017). Aggregation of a hepatitis C virus replicase module induced by ablation of p97/VCP. J. Gen. Virol. *98*, 1667–1678.

Yu, G.Y., Lee, K.J., Gao, L., and Lai, M.M.C. (2006). Palmitoylation and polymerization of hepatitis C virus NS4B protein. J. Virol. *80*, 6013–6023.

Zhang, C., Cai, Z.H., Kim, Y.C., Kumar, R., Yuan, F.H., Shi, P.Y., Kao, C., and Luo, G.X. (2005). Stimulation of hepatitis C virus (HCV) nonstructural protein 3 (NS3) helicase activity by the NS3 protease domain and by HCV RNA-dependent RNA polymerase. J. Virol. *79*, 8687–8697.

Zhang, Y., Zhao, X., Zou, J., Yuan, Z., and Yi, Z. (2019a). Dual role of the amphipathic helix of hepatitis C virus NS5A in the viral polyprotein cleavage and replicase assembly. Virology *535*, 283–296.

Zhang, Y., Zou, J.Y., Zhao, X.M., Yuan, Z.H., and Yi, Z.G. (2019b). Hepatitis C virus NS5A inhibitor daclatasvir allosterically impairs NS4B-involved protein-protein interactions within the viral replicase and disrupts the replicase quaternary structure in a replicase assembly surrogate system. J. Gen. Virol. *100*, 69–83.

STAR★METHODS

KEY RESOURCES TABLE

REAGENT or RESOURCE	SOURCE	IDENTIFIER
Antibodies		
Mouse monoclonal anti-NS5A	Gifted by Charles Rice from Rockefeller University	N/A
Mouse monoclonal anti-NS3	Virogen	Cat#217-A
Rat monoclonal anti-HA	Roche	Cat#11867423001; RRID:AB_390919
Rabbit monoclonal anti-Myc	Cell Signaling Technology	Cat#2278; RRID:AB_490778
Goat-anti-rat HRP IgG	Santa Cruz	Cat#sc-2005
Goat-anti-mouse IRDye 800CW IgG	Licor	Cat#926-32210; RRID:AB_621842
Goat-anti-rabbit IRDye 800CW IgG	Licor	Cat#926-32211; RRID:AB_621843
Bacterial and virus strains		
sgJFH1-sGluc	(Zhang et al., 2019a)	N/A
Chemicals, peptides, and recombinant proteins		
4-Azido-L-phenylalanine (azF)	MedChemExpress	Cat# HY-16714
Anti-HA magnetic beads	ThermoFisher Scientific	Cat#88837; RRID:AB_2861399
Renilla luciferase assay system	Promega	Cat#E2820
MEGAscript T7 Transcription Kit	Invitrogen	Cat#AM1334
TransIT-LT1 Reagent	Mirus	Cat#MIR2306
TransIT-mRNA kit	Mirus	Cat#MIR2250
Experimental models: cell lines		
HEK293T	Cell Bank of the Chinese Academy of Sciences	Cat#SCSP-502
Huh7.5	Gifted by Charles Rice from Rockefeller University	N/A
Oligonucleotides		
Primers for plasmid construction	This paper	Table S3
Recombinant DNA		
pSVB.Yam	Gifted by Thomas P. Sakmar from Rockefeller University	N/A
pcDNA.RS	Gifted by Thomas P. Sakmar from Rockefeller University	N/A
pcDNA3.1-GST^{HA}	This paper	N/A
pcDNA3.1-GST^{HA}-V125-TAG	This paper	N/A
phCMV-Myc-MOB1b	This paper	N/A
phCMV-NS3-5B-5A^{HA}	(Zhang et al., 2019b)	N/A
phCMV-NS3-5B-5A^{HA} TAG mutants	This paper	Table S4
phCMV-NS3-5B-4B^{HA}	(Zhang et al., 2019b)	N/A
phCMV-NS3-5B-4B^{HA} TAG mutants	This paper	Table S4
phCMV-NS3-5B-4B^{HA} NS4B-K18-TAG-L237A	This paper	N/A
phCMV-NS3-5B-4B^{HA} NS4B-I21-TAG-L237A	This paper	N/A
phCMV-NS3-5B-4B^{HA}-L237A	This paper	N/A
phCMV-NS3-5B-4B^{HA}-L237-TAG-L17A	This paper	N/A
phCMV-NS3-5B-4B^{HA}-L237-TAG-L17A/K18A/S19A	This paper	N/A

(*Continued on next page*)

Continued

REAGENT or RESOURCE	SOURCE	IDENTIFIER
phCMV-NS3-5B-4B^{HA}-L237-TAG-L17A/K18A/S19A/K20A/I21A	This paper	N/A
phCMV-NS3-5B-5A^{HA}-NS5A-W84-TAG-F36A/I37A/S38A/R112A/E148A	This paper	N/A
phCMV-NS3-5B-5A^{HA} -NS5A-I15-TAG-F36A/I37A/S38A/R112A/E148A	This paper	N/A
phCMV-NS3-5B-4B^{HA}-NS5A-C13A	This paper	N/A
phCMV-NS3-5B-4B^{HA}-NS5A-T17A	This paper	N/A
phCMV-NS3-5B-4B^{HA}-NS5A-D18A	This paper	N/A
phCMV-NS3-5B-5A^{HA}-NS5A-W84-TAG-C13A	This paper	N/A
phCMV-NS3-5B-5A^{HA}-NS5A-W84-TAG-T17A	This paper	N/A
phCMV-NS3-5B-5A^{HA}-NS5A-W84-TAG-D18A	This paper	N/A
phCMV-NS3-5B-4B^{HA}-S227A/D228A/R232A	This paper	N/A
phCMV-NS3-5B-5A^{HA}- S227A/D228A/R232A	This paper	N/A
sgJFH1-sGluc-NS4B-L237A	This paper	N/A
sgJFH1-sGluc-NS4B-S227A	This paper	N/A
sgJFH1-sGluc-NS4B-D228A	This paper	N/A
sgJFH1-sGluc-NS4B-R232A	This paper	N/A
sgJFH1-sGluc-NS5A-W84A	This paper	N/A
Software and algorithms		
ImageJ	NIH	https://imagej.net/
Prism 6.0	GraphPad	https://www.graphpad.com/scientificsoftware/prism/
Adobe Photoshop	Adobe	https://www.adobe.com/products/photoshop.html
Adobe Illustrator	Adobe	http://www.adobe.com/products/illustrator.html
UCSF Chimera	UCSF	http://plato.cgl.ucsf.edu/chimera/

RESOURCE AVAILABILITY

Lead contact

Further information and requests for resources and reagents should be directed to and will be fulfilled by the Lead Contact, Zhigang Yi (zgyi@fudan.edu.cn).

MATERIALS AVAILABILITY

Plasmids generated in this study are available upon request from the Lead Contact.

Data and code availability

This study did not generate datasets or code.

EXPERIMENTAL MODEL AND SUBJECT DETAILS

Cell lines

The human embryonic kidney cell line HEK293T (the sex information was not available, Cell Bank of the Chinese Academy of Sciences, Shanghai, China, www.cellbank.org.cn) were routinely maintained in Dulbecco's modified medium supplemented with 10% FBS (Gibco) and 25mM HEPES (Gibco). Huh7.5 (the sex information was not available, kindly provided by Charles Rice from

Rockefeller University) were routinely maintained in Dulbecco's modified medium supplemented with 10% FBS (Gibco) and 25mM HEPES (Gibco) with non-essential amino acids (Gibco). All cell lines were incubated at 37°C in humidified environmental incubator with 5% CO2.

METHOD DETAILS

Plasmids

The suppressor tRNA plasmid (pSVB.Yam) and mutant amino-acyl tRNA synthetase plasmid for p-azido-L-phenylalanine (pcDNA.RS) (Ye et al., 2008) were kindly provided by professor Thomas P. Sakmar (Rockefeller University). The cDNA of *E. coli* GST with a fused N-terminal HA tag was synthesized and cloned into BamHI/EcoRI sites of pCDNA3.1 to get the plasmid pcDNA3.1-GST^{HA}. The V125-TAG was introduced into GST to get the plasmid pcDNA3.1-GST^{HA}-V125-TAG by fusion PCR-mediated mutagenesis. The MOB1b cDNA was cloned into BglII/NotI sites of phCMV with a fused N-terminal Myc tag to get the plasmid phCMV-Myc-MOB1b. Plasmid phCMV-NS3-5B-5A^{HA} and phCMV-NS3-5B-4B^{HA} have been described previously (Zhang et al., 2019b). TAGs were introduced into NS3-5B expressing plasmids by fusion PCR-mediated mutagenesis. The NS4B TAG mutants (amino acids 1-66, 80, 96, 162, 180, 128-136, 191-261) and NS5A TAG mutants (amino acids 1-30, 48, 84, 92, 94, 116, 149, 166, 312, 317, 322) were introduced into plasmid phCMV-NS3-5B-4B^{HA} or plasmid phCMV-NS3-5B-5A^{HA} by fusion PCR-mediated mutagenesis, respectively (Table S4). The NS4B L237A mutation was introduced into plasmid phCMV-NS3-5B-4B^{HA}-NS4B-K18-TAG, phCMV-NS3-5B-4B^{HA}-NS4B-I21-TAG and plasmid phCMV-NS3-5B-4B^{HA} to get the plasmid phCMV-NS3-5B-4B^{HA} NS4B-K18-TAG-L237A, phCMV-NS3-5B-4B^{HA}-NS4B-I21-TAG-L237A and the plasmid phCMV-NS3-5B-4B^{HA}-L237A, respectively. The NS4B L17A, L17A/K18A/S19A, L17A/K18A/S19A/K20A/I21A mutations were introduced into plasmid phCMV-NS3-5B-4B^{HA}-L237-TAG to get the plasmids phCMV-NS3-5B-4B^{HA}-L237-TAG-L17A, phCMV-NS3-5B-4B^{HA}-L237-TAG-L17A/K18A/S19A and phCMV-NS3-5B-4B^{HA}-L237-TAG-L17A/K18A/S19A/K20A/I21A, respectively. The NS5A F36A/I37A/S38A/R112A/E148A mutations were introduced into the plasmids phCMV-NS3-5B-5A^{HA}-NS5A-W84-TAG and phCMV-NS3-5B-5A^{HA}-NS5A-I15-TAG to get the plasmids phCMV-NS3-5B-5A^{HA}-NS5A-W84-TAG-F36A/I37A/S38A/R112A/E148A and phCMV-NS3-5B-5A^{HA} -NS5A-I15-TAG-F36A/I37A/S38A/R112A/E148A, respectively. NS5A C13A, T17A, D18A mutations were introduced into plasmid phCMV-NS3-5B-4B^{HA} to get plasmids phCMV-NS3-5B-4B^{HA}-NS5A-C13A, phCMV-NS3-5B-4B^{HA}-NS5A-T17A, phCMV-NS3-5B-4B^{HA}-NS5A-D18A, respectively. NS5A C13A, T17A, D18A mutations were introduced into plasmid phCMV-NS3-5B-5A^{HA}-NS5A-W84-TAG to get the plasmids phCMV-NS3-5B-5A^{HA}-NS5A-W84-TAG-C13A, phCMV-NS3-5B-5A^{HA}-NS5A-W84-TAG-T17A and phCMV-NS3-5B-5A^{HA}-NS5A-W84-TAG-D18A, respectively. NS4B S227A/D228A/R232A were introduced into plasmids phCMV-NS3-5B-4B^{HA} and phCMV-NS3-5B-5A^{HA} to get the plasmids phCMV-NS3-5B-4B^{HA}-S227A/D228A/R232A and phCMV-NS3-5B-5A^{HA}- S227A/D228A/R232A, respectively. Plasmid sgJFH1-sGluc and sgJFH1-sGluc GND were described previously (Zhang et al., 2019a). NS4B L2237A, NS4B S227A, NS4B D228A, NS4B R232A, NS5A W84A were introduced into sgJFH1-sGluc to get the plasmids sgJFH1-sGluc-NS4B-L237A, sgJFH1-sGluc-NS4B-S227A, sgJFH1-sGluc-NS4B-D228A, sgJFH1-sGluc-NS4B-R232A, and sgJFH1-sGluc-NS5A-W84A, respectively. All the plasmids were proofed by Sanger DNA sequencing. The details of plasmids were described in Table S4.

Antibodies and compounds

Anti-NS5A monoclonal antibody (9E10; gifted by Charles Rice) was used at 1:1,000 dilution; Anti-NS3 monoclonal antibody (Virogen; 217-A) was used at 1:1,000 dilution; Anti-HA antibody (Roche; 11867423001) was used at 1:000 dilution; Anti-Myc antibody (Cell signaling technology; 2278) was used at 1:000 dilution; Goat-anti-rat HRP IgG (Santa Cruz; sc-2005) was used at 1:2,000 dilution; Goat-anti-mouse IRDye 800CW secondary antibody (licor; 926-32210) was used at 1:10,000 dilution; Goat-anti-rabbit IRDye 800CW secondary antibody (licor; 926-32211) was used at 1:10,000 dilution. 4-Azido-L-phenylalanine (azF) was purchased by MedChemExpress (HY-16714) and dissolved in pre-warmed cell culture media before use.

In-vivo photocrosslinking

Photocrosslinking was performed according to a previously reported protocol with modifications (Naganathan et al., 2013). Briefly, 1 × 10^6 HEK293T cells on 6-well plates were cotransfected with 1 μg of plasmids containing the amber stop codon at the desired position, 1μg suppressor tRNA cDNA (pSVB.Yam) and 0.1μg mutant amino-acyl tRNA synthetase cDNA for p-azido-L-phenylalanine (pcDNA.RS) by TransIT-LT1 (Mirus) at a ratio of 1:3 (plasmid: reagent). Six hours after transfection, the medium was changed to DMEM containing 20% FBS and 1 mM azF. The next day, the growth media was replaced with DMEM containing 10% FBS and 0.5 mM azF. Forty-eight hours posttransfection, the cells were washed with PBS and then photocrosslinked by exposure to 365 nm UV light with a UV lamp (WFH-204B, Shanghai Jingke) in a dark room on ice for 30 min. Then, the cells were either directly harvested by 2× SDS loading buffer for Western blot analysis or lysed in IP buffer for immunoprecipitation.

Western blotting

After washing with PBS, cells were lysed with 2× SDS loading buffer (100 mM Tris-Cl [pH 6.8], 4% SDS, 0.2% bromophenol blue, 20% glycerol, 10% 2-mercaptoethanol) and then boiled for 5 min. Proteins were separated by SDS-PAGE and transferred to a nitrocellulose membrane. The membranes were incubated with blocking buffer (PBS, 5% milk, 0.05% Tween) for 1 hour and then with a primary antibody diluted in blocking buffer. After three washes with PBST (PBS, 0.05% Tween), the membranes were incubated with a secondary antibody. After three washes with PBST, the membrane was visualized by Western Lightning Plus-ECL substrate

(PerkinElmer, NEL10500) or by an Odyssey CLx Imaging System. The protein bands were quantified by densitometry with ImageJ as necessary.

Immunoprecipitation

Cells in 6-well plates were lysed with 150 μl lysis buffer (50 mM TrisCl [pH 7.5], 1 mM EDTA, 15 mM $MgCl_2$, 10 mM KCl, 1% Triton X-100, proteinase inhibitor [Roche]). Then, cell lysates were passed through a 27-gauge needle 20 times and centrifuged at 12000 ×*g* for 10 min. Fifteen microliters of the supernatant was taken and mixed with an equal volume of 2 × SDS loading buffer as input (10%). The rest of the clarified cell lysates were incubated with 10 μl anti-HA magnetic beads (Pierce, SB246262) overnight with rotation at 4°C. After four washes with wash buffer (50 mM TrisCl [pH 7.5], 1 mM EDTA, 15 mM MgCl2, 10 mM KCl, 1% Triton X-100), the beads were lysed with 2 × SDS loading buffer. The samples were boiled for 10 min and then analyzed by Western blotting.

In-vitro transcription

XbaI-linearized plasmids were purified and used as templates for the *in-vitro* transcription by using MEGAscript T7 Transcription Kit (Ambion) according to the manufacturer's protocol. The RNAs were purified by RNeasy Mini kit (Qiagen).

Transfection

For plasmid transfection, 1×10^6 HEK293T cells were seeded onto poly-L-lysine (Sigma)-coated 6-well plates and then transfected with plasmids using a TransIT-LT1 transfection kit (Mirus) according to the manufacturer's protocol. For RNA transfection, 6.25×10^4 Huh7.5 cells were seeded onto 48-well plates and then transfected with 0.25 μg *in-vitro*-transcribed RNA using a TransIT-mRNA transfection kit (Mirus) according to the manufacturer's protocol.

Luciferase activity

Supernatants were taken from cell medium and mixed with equal volume of 2 × lysis buffer (Promega). Luciferase activity was measured with Renilla luciferase substrate (Promega) according to the manufacturer's protocol.

QUANTIFICATION AND STATISTICAL ANALYSES

The protein bands of the immunoblots were quantified by densitometry with ImageJ. Data were analyzed with GraphPad Prism 6.0 software. Data are expressed as the mean ± standard deviation (SD) or mean ± standard error of mean (SEM). Comparisons of groups were performed using two tailed, unpaired *t*-test, *$p < 0.05$, **$p < 0.01$, ***$p < 0.001$, ****$p < 0.0001$.